Innovative Food Science and Emerging Technologies 34 (2016) 100–111

Contents lists available at ScienceDirect

Innovative Food Science and Emerging Technologies

journal homepage: www.elsevier.com/locate/ifset

A novel strategy for improving radio frequency heating uniformity of dry food products using computational modeling

Zhi Huang [a], Francesco Marra [b], Shaojin Wang [a,c,*]

[a] College of Mechanical and Electronic Engineering, Northwest A&F University, Yangling, Shaanxi 712100, China
[b] Dipartimento di Ingegneria Industriale, Università degli studi di Salerno, Fisciano, SA, Italy
[c] Department of Biological Systems Engineering, Washington State University, 213 L.J. Smith Hall, Pullman, WA 99164-6120, USA

ARTICLE INFO

Article history:
Received 8 December 2015
Received in revised form 8 January 2016
Accepted 10 January 2016
Available online 27 January 2016

Keywords:
Computer simulation
Dielectric properties
Heating uniformity
Radio frequency
Soybean flour

ABSTRACT

This study attempted to quantify effects of dielectric properties (DPs) and densities of a surrounding container and treated food products on heating uniformity in a 6 kW, 27.12 MHz parallel plate radio frequency (RF) system. A computer simulation model was established with finite element-based commercial software, COMSOL Multiphysics®, and experiments with 1.5 kg soybean flour packed in a rectangular polystyrene container were performed to validate the developed model. Surface temperature distributions of soybean flour in three different horizontal layers were obtained with an infrared camera, and temperature–time histories at two representative locations inside the container were monitored with two optical fiber sensors. The uniformity index (UI) was used as a criterion to evaluate the RF heating uniformity within food products. Results showed that the RF heating uniformity in food samples was clearly influenced by DPs and density of the surrounding container. UI was the lowest when the surrounding container dielectric constant was in a comparable range of the sample's, with the loss factor values of surrounding container lying between 0.01–0.1% of the sample's. The optimum RF heating uniformity in food products could be achieved with a smaller density value of the surrounding container. The correlations of DPs and density between surrounding container and food products derived from the validated simulation model could provide valuable information and strategy to improve the RF heating uniformity in low moisture foods for insect or microbial control. Thus, the established strategy can further be used for developing effective industrial-scale RF treatment protocols after optimization of this process by the food industry.

Industrial relevance: Although the most important characteristic of radio frequency (RF) treatments is fast and volumetric heating generated by dipole rotation and ionic conduction, edge over-heating is still a major problem for foods heated in rectangular containers. The validated model was used to study the effects of dielectric properties and density of sample and surrounding container on sample uniformity index. Simulated results illustrated that the RF heating uniformity could be improved when the dielectric constant and density of surrounding container and sample were in accordance with the established relationships. The established strategy may provide valuable optimized methods to ensure RF heating uniformity in industrial applications.

1. Introduction

Low moisture foods, such as wheat flour, corn meal, glutinous rice flour, nuts, spices, and milk powders, are normally considered as shelf stable foods and can be stored for a long time due to preventing bacterial growth in its low moisture environment. Soybean flour is a popular food due to its high nutritional value and functional characteristics, which contain flavonoids, fiber and bioactive peptides (Hassan, 2013). Pathogens and insect pests, however, are found to survive in a low moisture environment more easily for several months (Finn et al., 2013; Johnson, Wang, and Tang, 2010; Mohapatra, Kar, and Giri, 2015). The qualitative and quantitative losses can reach as high as 30% due to insect damages (FAOSTAT, 2013), which also promote mold growth, toxin production, and product degradation in low moisture foods (Jiao, Johnson, Tang, and Wang, 2012; Vijay, Bhuvaneswari, and Gajendran, 2015). Several cases of soybean flour contamination with *Plodia interpunctella* greatly affect the quality and taste properties of the endproduct made by the flour (Singh, Satya, and Naik, 2013). Radio frequency (RF) heating involves utilizing electromagnetic energy at a frequency range of 3 kHz to 300 MHz to heat target foods. It has been considered as a novel heating technology for controlling insect and microbial populations in several dry products, such as almond (Gao, Tang, Villa-Rojas, Wang, and Wang, 2011), date (Ben-Lalli, Bohuon, Collignan, and Méot, 2013), lentil (Jiao et al., 2012), raisin

* Corresponding author at: College of Mechanical and Electronic Engineering, Northwest A&F University, Yangling, Shaanxi 712100, China. Tel.: +86 29 87092391; fax: +86 29 87091737.
E-mail address: shaojinwang@nwsuaf.edu.cn (S. Wang).

http://dx.doi.org/10.1016/j.ifset.2016.01.005
1466-8564/

Notation

Ave	average
α	thermal diffusivity ($m^2\ s^{-1}$)
C_p	heat capacity ($J\ kg^{-1}\ K^{-1}$)
E	electric field intensity ($V\ m^{-1}$).
$\vec{E}$	the electric field vector ($V\ m^{-1}$)
f	frequency (Hz)
h	heat transfer coefficient ($W\ m^{-2}\ K^{-1}$)
i	the data node number
I_a	the measured anode current (A)
k	thermal conductivity ($W\ m^{-1}\ K^{-1}$)
$\vec{n}$	the normal vector (dimensionless)
N	the total number of data points
P	power density generated by electric field ($W\ m^{-3}$)
SD	standard deviation
t	time (s)
T	sample temperature (K)
V	electric potential (V)
V_{vol}	sample volume (m^3)
ε	permittivity of the load ($F\ m^{-1}$)
ε_0	free space permittivity ($F\ m^{-1}$)
ε'	dielectric constant (dimensionless)
ε''	dielectric loss factor (dimensionless)
∇	gradient operator
ρ	density ($kg\ m^{-3}$)

Subscripts

a	air
exp	experiment
ini	initial
sim	simulation
t	target
vol	volume

(Alfaifi et al., 2014), spice (Kim, Sagong, Choi, Ryu, and Kang, 2012), and wheat (Jiao, Deng, Zhong, Wang, and Zhao, 2015).

Although the most important characteristic of RF treatments is fast and volumetric heating generated by dipole rotation and ionic conduction, edge over-heating is still a major problem for foods heated in rectangular containers (Alfaifi et al., 2014; Tiwari, Wang, Tang, and Birla, 2011a, 2011b). Edges and corners always absorb more electromagnetic energy compared to other regions due to different dielectric properties (DPs) between food products and the surrounding media (usually air), resulting in an uneven electric field distribution (Birla, Wang, Tang, and Hallman, 2004). The non-uniform heating in RF treated products may cause either survivals of pathogens/insects or degraded quality (Birla et al., 2004; Jiao et al., 2012; Kim et al., 2012). A number of methods have been reported for overcoming non-uniform RF heating, such as combination with an external heating or cooling (Birla et al., 2004; Hou, Ling, and Wang, 2014; Wang, Tiwari, Jiao, Johnson, and Tang, 2010), enclosing in another medium (Ikediala, Hansen, Tang, Drake, and Wang, 2002; Jiao, Tang, and Wang, 2014), mixing or rotating food (Birla et al., 2004; Chen, Wang, Li, and Wang, 2015), modifying electrode shapes (Tiwari et al., 2011a; Alfaifi et al., 2014), and sample movement (Hou et al., 2014). The trial and error procedures are time consuming, costly, and often provide limited information, which cannot easily identify the mechanism behind non-uniform RF heating. Finite element modeling may serve as valuable tools to acquire deep insights on the heating uniformity of products and offer opportunity to clearly understand RF interactions with food components without the necessity of extensive experiments.

Modeling RF processes is a multi-physics problem that involves the solution of coupled electromagnetic and heat transfer equations. Several simulation models have been developed to improve the RF heating uniformity for different food materials, such as apple (Birla et al., 2004), fish (Llave, Liu, Fukuoka, and Sakai, 2015), meat batters (Marra, Lyng, Romano, and McKenna, 2007), peanut butter (Jiao, Shi, Tang, Li, and Wang, 2015), raisins (Alfaifi et al., 2014), shell eggs (Lau, 2015), soybeans (Huang, Zhu, Yan, and Wang, 2015), wheat flour (Tiwari et al., 2011a, 2011b), and wheat kernels (Jiao, Deng, et al., 2015). The simulated uniformity index (UI) has been used as criteria to evaluate the temperature uniformity in RF treated products (Alfaifi et al., 2014; Huang, Zhu, Yan, et al., 2015; Jiao, Deng, et al., 2015; Tiwari et al., 2011a). Simulated results show that the RF heating uniformity could be improved by immersing the model fruit in water, suggesting that the non-uniform heating is mainly caused by the difference between DPs of food and its surrounding medium (Birla et al., 2004; Huang, Zhang, Marra, and Wang, 2016; Jiao, Tang, Wang, and Koral, 2014). When the dielectric constant of surrounding material is in a comparable range with the sample, the best heating uniformity would be achieved (Tiwari et al., 2011a; Huang, Zhu, Yan, et al., 2015). The dielectric constant determines the electric field distribution when the loss factor is far smaller than the dielectric constant (Jiao, Tang, and Wang, 2014, Jiao, Tang, Wang, et al., 2014; Metaxas, 1996). Following this approach, Jiao, Shi, et al. (2015) have shown that the temperature uniformity in peanut butter has been improved by minimizing the difference of dielectric constant between food sample and surrounding material. The temperature uniformity is greatly improved by placing soybean samples in a polystyrene container, which has the closest dielectric constant to that of soybeans and a lower dielectric loss factor value, as discussed in a recent study (Huang et al., 2016). Based on the study conducted by Huang et al. (2016), the container material, thickness, and corner radius have a significant effect on heating uniformity of soybeans during RF processes. Hence, the best combination of parameters in adjusting the thickness and corner radius of the polystyrene container has been established for heating uniformity improvement. However, there is no available mathematical modeling in literature to identify the specific relationship of DPs between surrounding material and treated products for RF heating uniformity improvement. Therefore, it is desirable to conduct a numerical analysis to systematically study the RF heating characteristics and design treatment protocols to improve RF heating uniformity in low moisture foods.

The objectives of the current study were to: (1) develop a computer simulation model to predict the electric field intensity and temperature distribution in three different layers of soybean flour in a rectangular shaped container, (2) conduct experiments with soybean flour in a 6 kW, 27.12 MHz RF system to verify the simulation results, (3) apply the validated model to evaluate the heating uniformity of soybean flour influenced by DPs and density of the surrounding container and treated products, and (4) establish the DP and density correlations between surrounding container and treated food sample when the best heating uniformity was obtained.

2. Materials and methods

2.1. Raw material preparation

Soybean flour (*Glycine max*) was purchased from a local market in Yangling, Shaanxi, China. A total of 20 kg of soybean flour was kept in polyethylene bags and stored at a constant temperature (20 °C) in a thermostatic and humidity (50% RH) controlled chamber (BSC-150, Shanghai BoXun Industrial & Commerce Co., Ltd., Shanghai, China). They were taken out from the chamber and kept at ambient room temperature (20 ± 1 °C) for 4 h prior to RF processing. The initial moisture content of tested soybean flour was 7.93 ± 0.08% on wet basis (w.b.).

Table 1
Electrical and thermo-physical properties of materials used in computer simulation.

Property	Electrode[a]	Air[a]	Polystyrene[b]	Soybean flour
Density (ρ, kg m^{-3})	2700	1.2	25	380
Specific heat (C_p, J kg^{-1} K^{-1})	900	1000	1300	$5.8 \cdot T + 1614$
Thermal conductivity (k, W m^{-1} K^{-1})	160	0.026	0.036	$0.0007 \cdot T + 0.083$
Dielectric constant (ε')	1	1	2.6	3.96[c]
Loss factor (ε'')	0	0	0.0003	0.38[c]

Source: T = temperature (°C).
[a] COMSOL Material Library, V4.2a (2012).
[b] Huang et al. (2016).
[c] Guo et al. (2010).

2.2. Container material and dimensions

The polystyrene container was chosen based on the closest dielectric constant to that of soybean flour with a small dielectric loss factor (Table 1). With the main advantage of lower density, cheap, stable, high heat resistance and portable characteristics, polystyrene is widely used in the food processing and packaging industry. The inner dimension of the rectangular polystyrene container was 30 L × 22 W × 6 H cm^3 (Fig. 1), and the thickness for the bottom and side walls was fixed at 2 cm (Huang et al., 2016).

2.3. Temperature measurements

About 1.5 kg soybean flour samples filled the rectangular container and were horizontally divided into three layers (A: z = 6 cm; B: z = 4 cm; C: z = 2 cm) parallel to the container bottom by two thin polypropylene films (mesh opening of 0.2 mm) with each filled of 0.5 kg to represent the temperature distribution inside the sample (Fig. 1). An infrared camera (DM63-S, DaLi Science and Technology Co., Ltd, Zhejiang, China) with an accuracy of ±2 °C was used for mapping surface temperatures of soybean flour in three different layers after RF treatment. The thermal digital infrared camera was first calibrated against a thin thermocouple thermometer (HH-25TC, Type-T, OMEGA Engineering Inc., Stamford, Connecticut, USA) with an accuracy of ±0.5 °C and 0.9 s response time. For internal temperature monitoring during RF heating, two optical fiber sensors (1.8 mm diameter) attached to a temperature measurement system (FTS-P104, Xi'an HeQi Opo-Electronic Technology Co., Ltd, Shaanxi, China) were inserted at the center (B_1) and near the corner (B_2) at the middle layer (z = 4 cm) of food sample. The optical fiber sensors were calibrated by using an ice–water mixture and boiling water before experiment and temperatures were recorded at 1 s intervals. A plastic foam board (29 L × 21 W × 2 H cm^3) made from polystyrene was used to cover the top of the container. The sensors were inserted at the center (B_1) and corner (B_2) of the board using a drill to ensure precise hole positioning (Fig. 1). These positions were held by fixing the sensor cables to a stationary position through the feeding inlet of the RF machine.

2.4. Computer modeling of RF heating

2.4.1. Physical model

A 6 kW, 27.12 MHz free running oscillator pilot scale RF system (COMBI 6-S, Strayfield International Limited, Wokingham, UK) was used in this study (inner dimension 129 × 109 × 52 cm^3). This system consisted of a chamber with electrically insulated walls and two parallel rectangular electrodes, a generator, power amplifier, matching unit, and a RF applicator. The RF power was set automatically by controlling the voltage to the power amplifier from the generator, which was fed in the middle of the top electrode back-side and proportional to the electrode gap by changing the top electrode position with the aid of adjustable screws (Fig. 2). A 1-cm-thick polystyrene sheet with the area of 83 × 40 cm^2 (same as the top electrode) was placed above the bottom electrode to prevent direct contact between the electrode and the container. The polystyrene container with a bottom thickness of 2 cm was placed in the center of the polystyrene sheet for achieving better RF heating uniformity (Huang, Zhu, Yan, et al., 2015; Tiwari et al., 2011a; Jiao, Deng, et al., 2015). To ensure repeatability of the experimental results and limit the influence of non-uniform electromagnetic fields on sample, the location of the sample was fixed on the center and middle between the top and bottom electrodes during all experiments (Llave et al., 2015).

2.4.2. Governing equations

The electric field distribution within the load (food sample and the container) and at any point inside the electrodes was given by the

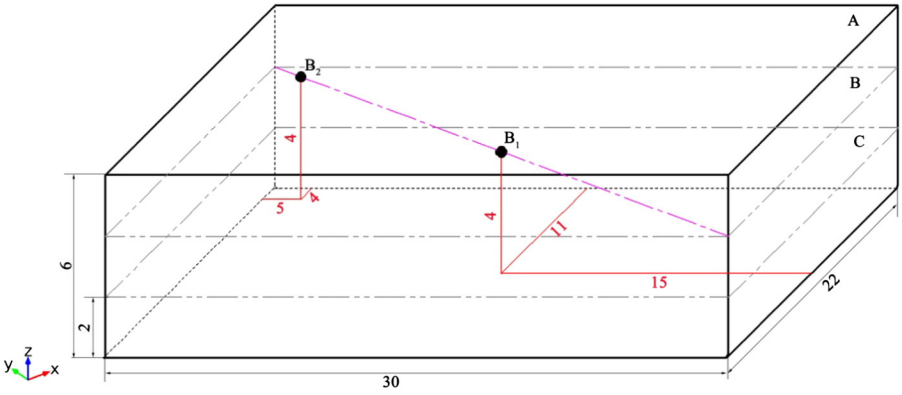

Fig. 1. Position of two optical fiber temperature sensors in the rectangular polystyrene container split into three layers (A—top, B—middle, C—bottom layer) for temperature profile measurements (all measures in cm).

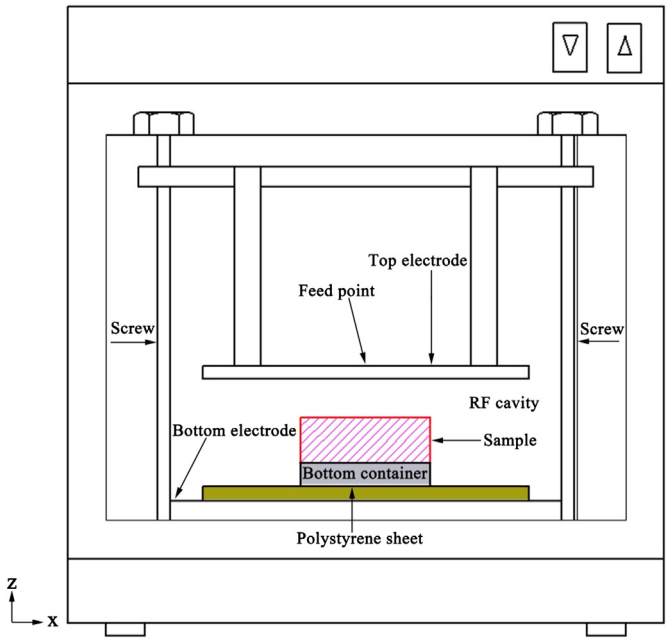

Fig. 2. Schematic diagram of the 6 kW, 27.12 MHz RF system.

solution of the Gauss law derived from a quasi-static approximation of Maxwell's equations (Marra et al., 2007):

$$\vec{\nabla}\left(\varepsilon \cdot \vec{E}\right) = 0 \tag{1}$$

where ε is permittivity of the load and $\vec{E}$ is the electric field vector. Simulation of RF heating as a quasi-static electric field between the electrodes was preferred since the wavelength (11 m) in the 27.12 MHz RF system is often much larger than the analyzed domain sizes.

The RF power conversion to thermal energy (P, W m^{-3}) within the food sample under an electric field intensity ($|\vec{E}|$, V m^{-1}) are described as follows (Metaxas, 1996):

$$P = 2\pi f \varepsilon_0 \varepsilon'' \left|\vec{E}\right|^2 \tag{2}$$

where f is the frequency (Hz), ε_0 is the permittivity of electromagnetic wave in free space (8.86×10^{-12} F m^{-1}), ε'' is the relative dielectric loss factor of the sample load, and $|\vec{E}|$ is the modulus of the $E(x, y, z)$ field, the scalar voltage potential (V) is related to the electric field as $\vec{E} = -\vec{\nabla} V$.

The heat equation was solved within the food material and the container, considering the internal conduction and the heat generation due to RF energy, while external convection at the sample surface was taken into account in the boundary conditions. Therefore, the temperature distribution was simulated based on a 3D heat transfer equation, including solution of Fourier heat transfer equation plus a generation term, coupled with the quasi-static electro-magnetic field equations (Uyar et al., 2015):

$$\frac{\partial T}{\partial t} = \alpha \cdot \vec{\nabla}^2 T + \frac{P}{\rho C_p} \tag{3}$$

where ρ is density (kg m^{-3}), C_p is specific heat (J kg^{-1} K^{-1}), α is the thermal diffusivity (m^2 s^{-1}), T is the temperature (K), and t is the time (s). While the solution of heat transfer is needed just within the sample, the Gauss law must be evaluated for the space between the two electrodes, which includes the sample and the air around it (Marra et al., 2007).

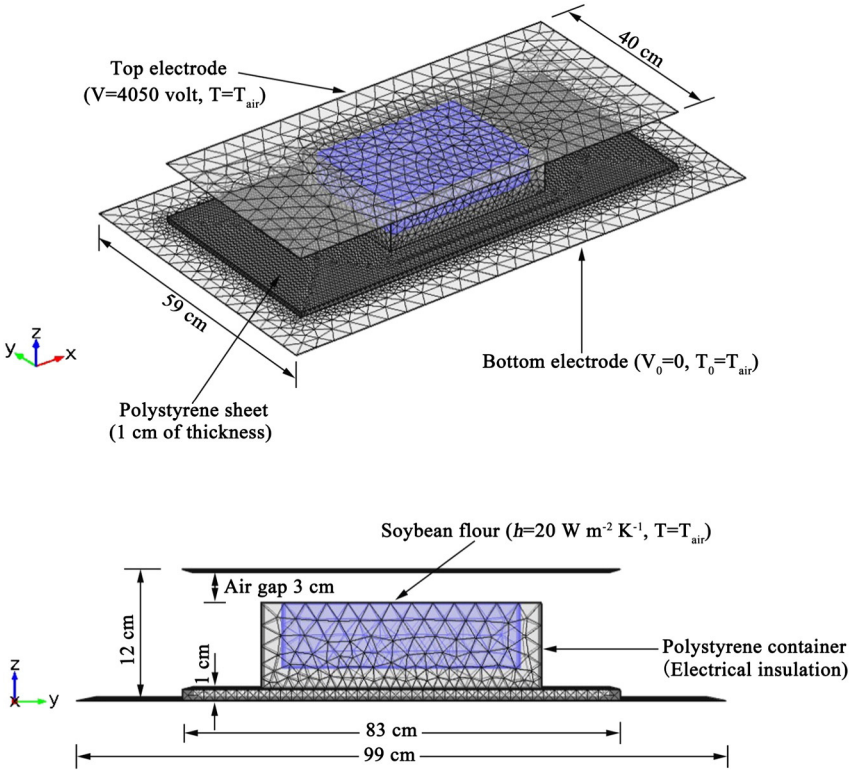

Fig. 3. 3-D model approach of the RF heating system used in simulations (mesh of 5 mm).

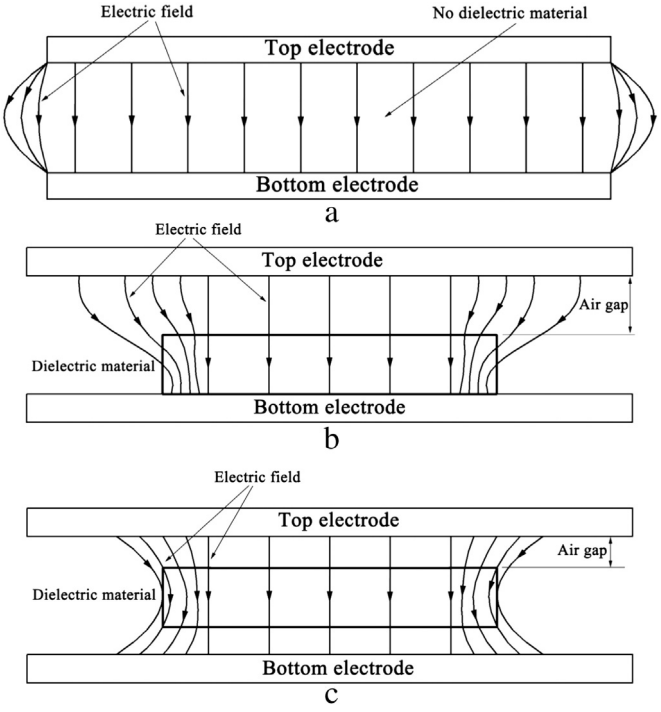

Fig. 4. The electric field strength between two parallel plate electrodes with (a) no dielectric sample, (b) dielectric sample placed on the center of bottom electrode, and (c) dielectric sample placed in the center and middle between top and bottom electrodes with a fixed electrode gap of 12 cm and initial temperature of 20 °C.

2.4.3. Geometric model

The 3D geometric model was developed using COMSOL (V4.3a COMSOL Multiphysics, COMSOL, Co., Ltd., Shanghai, China) based on the actual structure and size of the 6 kW, 27.12 MHz RF system (Fig. 3). The complete geometric model included RF cavity (129 × 109 × 52 cm^3), top (83 × 40 cm^2) and bottom electrode (99 × 59 cm^2), polystyrene sheet (83 × 40 × 1 cm^3), soybean flour sample (30 × 22 × 6 cm^3), and polystyrene container (34 × 26 × 8 cm^3) as shown in Fig. 3. Soybean flour samples were placed in the center and middle between the top and bottom electrodes with an air gap of 3 cm. The whole domain in this study was divided into three sub-domains, the food sample (SD1), container (SD2), and the surrounding air (SD3). In SD1 and SD2, both heat transfer and Gauss law equations were solved, whereas in SD3 only the dielectric phenomenon was considered. An unstructured mesh consisting of Lagrange quadratic elements was created over the entire domain of RF cavity. The extremely fine mesh structure was preferred based on the convergence tests even though it led to longer computational times, which consists of 122,868 domain elements (tetrahedrons), 10,574 boundary elements (triangles) and 879 edge elements (linear). The top electrode was drawn as an embedded element (work plane) in 3D to avoid a large number of mesh elements for a thin electrode plate. The *X*, *Y*, and *Z* directions were modeled using a mesh spacing of 5 mm, which provided satisfactory spatial resolution for the considered domain and the solution was found to be independent of the grid size with further refinement.

2.4.4. Thermo-physical and dielectric properties

The moisture content of soybean flour was determined by drying triplicate 3–5 g flour samples in aluminum moisture dishes in an oven (DZX-6020B, Shanghai Nanrong Co. Ltd., Shanghai, China) at 130 °C for 1 h until a substantially constant weight was obtained (AOAC, 2002). The density of soybean flour was calculated from the measured mass and volume at room temperature over three replicates. The specific heat and thermal conductivity of soybean flour were measured using a differential scanning calorimeter (DSC, Q2000, TA Instruments, New Castle, PA, USA). An empty sealed aluminum pan was used as a reference and 10 mg soybean flour samples were sealed in another aluminum pan (20 μL). The procedure included cooling the sample from room temperature to 0 °C, equilibrating for 6 min, and then heated in the DSC at a rate of 10 °C/min over a temperature range of 20–80 °C. Each measurement was repeated three times and details of the measurement system and procedure can be found elsewhere (Jiao, Tang, Wang, et al., 2014). These data were subjected to linear regression analysis for using these properties in simulation model over the treatment temperatures range from 20 to 60 °C (suitable for postharvest pest control). Dielectric properties of the soybean flour sample were reported at 27 MHz and the average dielectric constant and loss factor values were used in the simulation (Guo, Wang, Tiwari, Johnson, and Tang, 2010). The same method with constant dielectric properties has been used in simulations of wheat flour and peanut butter (Jiao, Tang, and Wang, 2014; Jiao, Tang, Wang, et al., 2014; Tiwari et al., 2011b). Dielectric and thermo-physical properties of the electrode and ambient air at room temperature (20 °C) were adapted from COMSOL material library (Table 1).

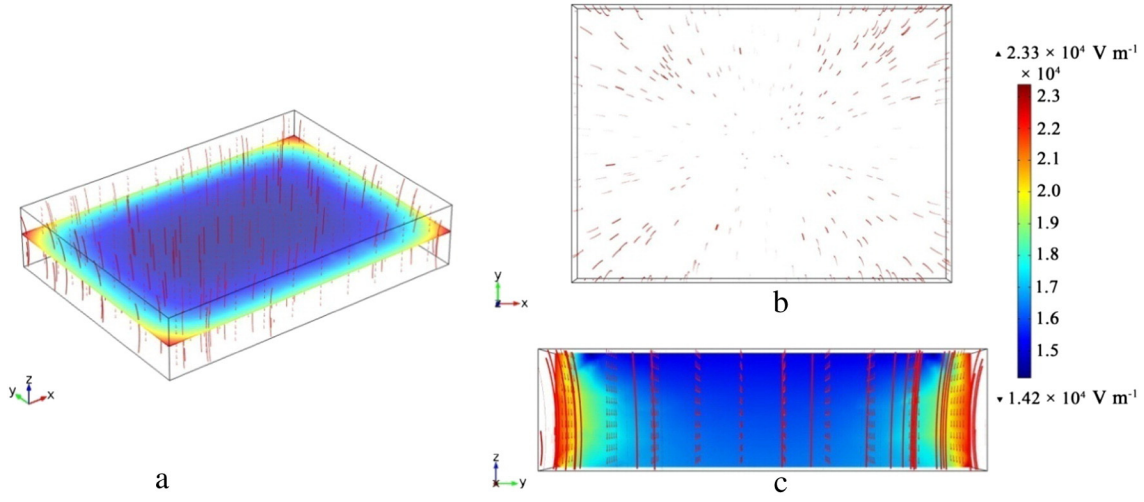

Fig. 5. Simulated electric field direction (arrow), electric field intensity (color surface, V m^{-1}), and electric potential (streamline) of soybean flour (30 × 22 × 6 cm^3) in (a) middle layer of whole sample ($z = 4$ cm), (b) top horizontal layer ($z = 6$ cm), and (c) vertical ($x = 11$ cm) center cross sections after 5 min RF heating with an electrode gap of 12 cm and initial temperature of 20 °C.

2.4.5. Initial and boundary conditions

The Gauss law needs boundary conditions for the electrodes and the RF cavity walls to determine the electric field distribution inside the system.

- The top electrode was set as the electromagnetic source since it introduced high frequency electromagnetic energy from the generator to the heating cavity, which maintained a certain potential V and constant during the processing time.
- All the metal shielding parts except for the top electrode were maintained at the ground condition ($V_0 = 0$).
- The metallic RF cavity walls and the plastic container were assumed to be electrically insulated ($\nabla \cdot \vec{E} = 0$), and for the left and right sides of the system, the surrounding air was considered.

For the heat transfer equation to determine the temperature distribution inside the system:

- The initial temperature of the two electrodes, surrounding air, polystyrene sheet, and polystyrene container was set at room temperature (20 °C), and the initial average temperature of the soybean flour was assumed at a uniform temperature ($T_0 = 20$ °C).
- The load was considered to be subjected to heat exchange with surrounding air by convection expressed as:

$$-k\vec{\nabla}T\vec{n} = h(T - T_a). \tag{4}$$

Heat exchange was approximated by assuming a convective heat transfer coefficient ($h = 20$ W m^{-2} K^{-1}, which is a typical value used for natural convection in air in the used configuration), k is thermal conductivity (W m^{-1} K^{-1}), T_a is the air temperature inside the RF cavity (20 °C) and $\vec{n}$ is the normal vector.

2.4.6. Constant electric potential

Even though the voltage varies all over the surface of the top electrode, it was assumed to be uniform since the electrode dimensions (0.83 × 0.4 m^2) were much lower than 30% of the RF wavelength (≈11 m). Thus, the calculation with constant electric potential applied at the top electrode was performed by the following equation with the measured anode current (I_a,A) (Zhu, Huang, and Wang, 2014):

$$V = 11242 \times I_a + 2029.9. \tag{5}$$

On the basis of the measured anode current (0.18 A), the top electric voltage applied was set at 4050 V for subsequent simulations. Based on our preliminary results, the voltage V varies up to 11% between standby and full-load conditions while Marshall and Metaxas (1998) reported that the difference was only 7%. Llave et al. (2015) also reported similar heating problems associated with the free-running oscillator systems.

2.4.7. Model assumptions

In the current simulation study, the following assumptions were considered to simulate temperature distribution of soybean flour subjected to RF heating:

- DPs and TPs (thermo-physical properties) of soybean flour were assumed to be homogeneous and isotropic, the density and dielectric properties were assumed as temperature independent.
- The mass and momentum transfers of water were ignored due to a short RF heating time (5 min) and the influence on moisture content was unnoticeable (<2%) based on preliminary study (Chen et al., 2015; Jiao, Deng, et al., 2015).

2.4.8. Solution methodology

The Joule heating module of a finite element based software COMSOL was used to solve this multi-physics problem that involves the solution of electromagnetic equation coupled with heat transfer equations. The important stages of the computer simulation included defining transport equations or domain and sub-domains of interest, describing dielectric and thermo-physical properties, setting up boundary conditions, meshing of the domains, and choosing the final numerical solver. All computer simulations were performed on a Dell workstation with an Intel® Core™ i5-2400, 3.10-GHz processor and 8 GB RAM running a Windows 8.1 64-bit operating system. The maximum and minimum mesh element sizes were 0.0578 m and 0.000578 m, respectively. Time step was determined by the max iteration per time step. If the computations were convergent before the max iteration, the time step could be short and would start the next iteration automatically. Based on extensive testing, the maximum iteration per time step was 10^4, and initial and maximum time steps were set as 0.001 and 1 s, respectively. The direct linear system solver UMFPACK was used for all calculations with a relative tolerance and an absolute tolerance of 0.01 and 0.001. Simultaneous solution of the coupled transient equations took nearly 5400 s (1.5 h) for simulating 300 s of the RF heating process at 1 s intervals.

2.5. RF experiments

In experiments, soybean flour samples with density of 380 kg m^{-3} were put into the rectangular container and positioned coaxially in the center and middle between the top and bottom electrodes of the RF system. The lethal temperature range for the complete mortality of

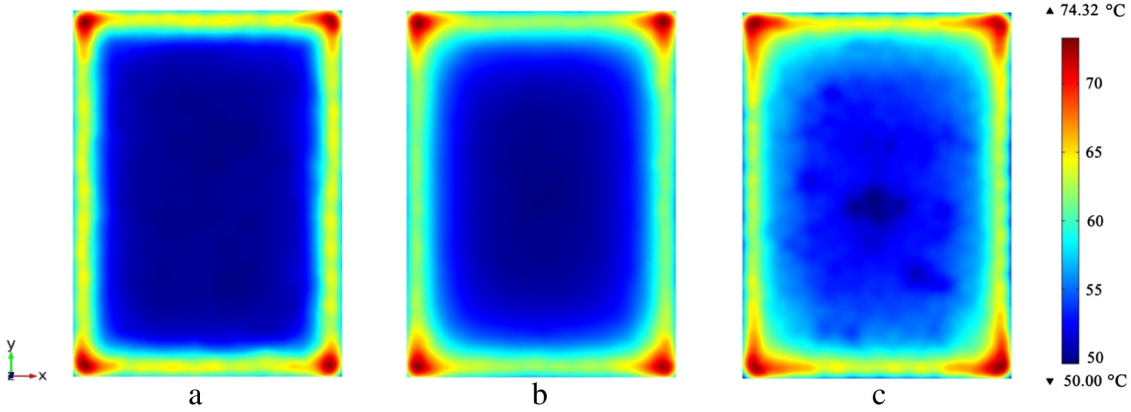

Fig. 6. Simulated temperature distributions (°C) at (a) top ($z = 2$ cm), (b) middle ($z = 4$ cm), and (c) bottom ($z = 6$ cm) layers of soybean flour ($30 \times 22 \times 6$ cm^3) placed in the center and middle between two electrodes after 5 min RF heating at an electrode gap of 12 cm and initial temperature of 20 °C.

many insects in soybean flour including *Indianmeal moth* at all life stages was within 44–52 °C with different holding times (Johnson, Wang, and Tang, 2003). To meet the required insect mortality and acceptable product quality, the soybean flour samples were subjected to RF heating for 5 min with an electrode gap of 12 cm according to our previously published RF power recommendations (Huang, Zhu, Yan, et al., 2015). Sample temperature–time histories at two representative locations in the middle layer of the soybean flour were measured using a six-channel optical fiber temperature measurement system with an accuracy of ±1 °C. Probes connected with two channels were inserted into the center and corner of soybean flour through predrilled holes while the remaining channels were used to monitor the air temperature inside the RF cavity (Fig. 1). Temperatures were sampled every second and recorded at 1 s intervals over 5 min. After 5 min RF heating, the container was immediately taken out from the RF cavity, and the surface temperature of soybean flour from top to bottom layer was measured by an infrared camera. All three thermal imaging recordings were completed in 20 s. The image analysis system (V1.0, DaLi Science and Technology Co., Ltd, Zhejiang, China) was used to collect and analyze the surface temperature data of soybean flour, and 97,856 individual temperature data were collected in each layer. The measured temperature profiles and the isothermal curves of soybean flour were used to validate the developed simulation model. Average and standard deviation values in the temperature of the RF heated samples were also compared over three layers.

2.6. Statistical analysis

Means and standard deviations were calculated with Sigma-Plot 12.0 (Systat Software, Inc., San Jose, CA, USA) statistical software. Sigma-Plot was used to perform t-test, one way analysis of variance (ANOVA) to identify difference among samples. To validate the simulation results, the root mean square error (RMSE) was calculated for the comparison of temperature differences between the simulated and experimental profiles over N time steps.

$$RMSE = \sqrt{\frac{1}{N}\sum_{i=1}^{N}\left[\left(T_{\exp}(i) - T_{sim}(i)\right)/T_{\exp}(i)\right]^2} \quad (6)$$

where T_{exp} and T_{sim} are the experimental and simulated temperatures (°C), respectively, i is the data node number, and N is the total number of points.

2.7. Heating uniformity evaluation

Cold spot locations were determined by finding the lowest temperature from thermal images and simulated temperature profiles, which were located at the center part of each layer (Huang, Chen, and Wang, 2015). In this study, all simulations were conducted based on the top surface center (cold spot) to reach the target disinfestation temperature (50 °C) after 5 min of RF heating. The relative sensitivity with respect to model inputs was evaluated using the temperature uniformity index (UI) inside the samples under the same electrode gap of 12 cm. It would reflect the degree to which temperature in the volume deviated from the target temperature (Jiao, Shi, et al., 2015):

$$UI = \frac{\int_{V_{vol}} \sqrt{(T - T_t)^2}\, dV_{vol}}{(T_t - T_{\text{ini}})V_{vol}} \quad (7)$$

where T_t and T_{ini} are the target and initial temperatures (°C) inside the dielectric material over the volume (V_{vol}, m^3). A smaller index corresponds to a better heating uniformity.

2.8. Simulation sequence

2.8.1. Simulation with varying DPs of the sample and container

The RF heating uniformity was significantly influenced by DPs of the treated material (Alfaifi et al., 2014; Huang, Zhu, and Wang, 2015). After the model was validated by comparing its results with the experimental ones, the computer simulation model was used to predict the effect of different parameters on RF heating uniformity in samples. To study the effect of container dielectric constant on UI of the sample, simulations were run by changing dielectric constant of the container from 0.1 to 19, with various sample dielectric constants ranging between 2 and 13. Electrode gap in each simulation was set at 12 cm with heating time of 5 min. The simulation voltage was determined when the lowest temperature at the top surface center (cold spot) to reach 50 °C (Jiao, Shi, et al., 2015). Another set of simulations were performed with

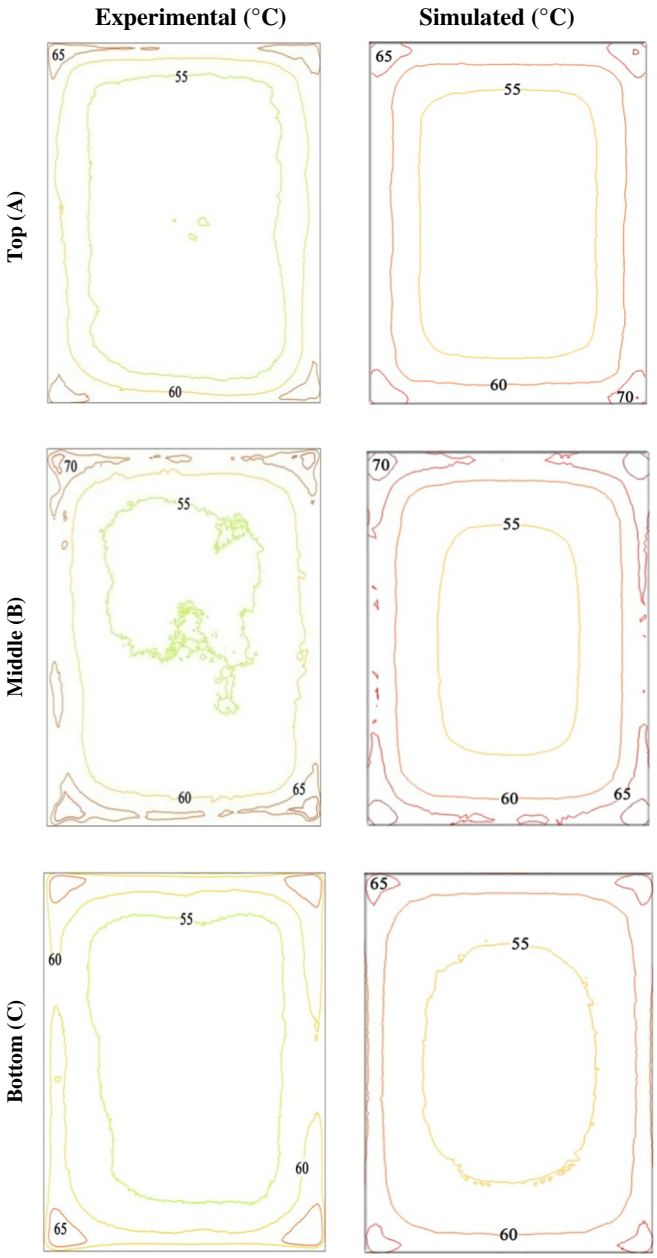

Fig. 7. Comparison of simulated and experimental temperature distributions (°C) in top (A), middle (B), and bottom layers (C) of soybean flour placed in a polystyrene container ($30 \times 22 \times 6$ cm^3) in the center and middle between the top and bottom electrodes after 5 min RF heating at a fixed electrode gap of 12 cm and initial temperature 20 °C.

container loss factor varied between 0.00003 and 0.3 and sample loss factor increased from 0.1 to 5 to study the effect of container loss factor on UI. Regression equations could be established for DPs of the sample and container based on the minimum UI values.

2.8.2. Simulation with varying density of sample and container

Since the specific heat and thermal conductivity had a relatively slight effect on RF heating uniformity based on previous studies (Huang, Zhu, and Wang, 2015; Tiwari et al., 2011b), a series of simulations were run by changing container density progressively between 20 and 1000 kg m^{-3}, while the density of the processed food was fixed as 300, 500, 800, and 1000 kg m^{-3}, respectively. Trends of the UI of soybean flour in each simulation were determined and the container density values corresponding to the minimum UI could be calculated using Matlab 2010 (Mathworks Inc., Natick, MA). Therefore, the density correlations between the surrounding container and treated products could be developed.

3. Results and discussions

3.1. Simulated electric field distribution for soybean flour

Fig. 4a–c show general trends of electric field distributions between two parallel plate electrodes without dielectric material, and with dielectric material placed on the bottom and middle between two electrodes. The electric field between two parallel plate electrodes was in parallel lines uniformly spaced throughout the region between two electrodes, and perpendicular to their surfaces with no dielectric material placed in it (Fig. 4a). When the dielectric material was placed at the center of the bottom electrode with an air gap over it, the presence of the surrounding air causes an intensification of the heating near the top of the electrode space at the edges of the material (Fig. 4b). This is in accordance with the report from Tiwari et al. (2011b), who found that sample in contact with either of the electrodes had higher RF power densities near the contact surfaces due to increased electric field concentration at those locations. This phenomenon has been reported in various food products treated in RF systems, such as the frozen lean beef sample (Uyar et al., 2015), fish (Llave et al., 2015), mung bean (Huang, Zhu, and Wang, 2015), peanut butter (Jiao, Tang, Wang, et al., 2014), and wheat (Chen et al., 2015). As observed in Fig. 4c, the electric field was distorted in the presence of the dielectric material placed in the middle of two parallel plate electrodes. Samples placed in the middle of RF electrodes showed higher electric field intensity at their central section as electric field deflected by both (top and bottom) edges with increased net electric field concentration at the central parts of the sample (Alfaifi et al., 2014; Tiwari et al., 2011a). Several analyses and investigations have been reported on the sample placement between two electrodes, confirming that the heating was more uniform when sample was placed in the middle of the two plate electrodes (Huang, Zhu, Yan, et al., 2015; Jiao, Tang, and Wang, 2014; Jiao, Deng, et al., 2015). This demonstrated the significant effect of surrounding material (usually air) on obtaining uniform electric field distributions inside the product.

Table 2
Comparison between simulated and experimental temperatures (Ave ± SD, °C) in three different horizontal layers of soybean flour placed in the center and middle between two electrodes after 5 min RF heating with an electrode gap of 12 cm and initial temperature of 20 °C.

Layer	Simulated (°C)	Experimental (°C)
	Ave ± SD	Ave ± SD
Top	57.9 ± 4.4aA*	56.8 ± 3.9aA
Middle	59.6 ± 5.4aA	58.8 ± 4.1aA
Bottom	56.8 ± 3.8aA	56.1 ± 3.2aA

* Mean values are not significantly different ($p > 0.05$) with the same lower and upper-case letters for different layers and treatments, respectively.

Fig. 5a–c show the simulated spatial E-field distributions of soybean flour in the middle layer of whole sample ($z = 4$ cm), top horizontal layer ($z = 6$ cm) and vertical ($x = 11$ cm) cross-section after the 5 min RF heating at a fixed electrode gap of 12 cm. In the whole 3-D model of the rectangular shaped sample, high electric field concentrations occurred at the corners and edges due to the refraction and reflection of the electrical field at these parts (Fig. 5b). Horizontally, electric field lines all bend at the interfaces between soybean flour and the contacted container side walls (Fig. 5a). As a result, net electric field increased at four sides and edges of the treated sample. In the vertical center cross-section ($x = 11$ cm), the electric field distribution was more uniform in the top and bottom than that in the other sections but concentrated at the side walls and center parts of the sample (Fig. 5c). The merging of two or more electric field lines at the edges and corners resulted in a higher volumetric power density, hence, overheating occurred in these areas more than that on the flat surfaces (Fu, 2004). The electric intensification was greater for samples either having a higher or lower dielectric constant than that for the surrounding materials (Huang, Zhu, Yan, et al., 2015; Tiwari et al., 2011a).

3.2. Simulated temperature profiles for soybean flour

The results presented in Fig. 5 showed that corners, edges, and middle parts had a higher electric field concentration when the sample

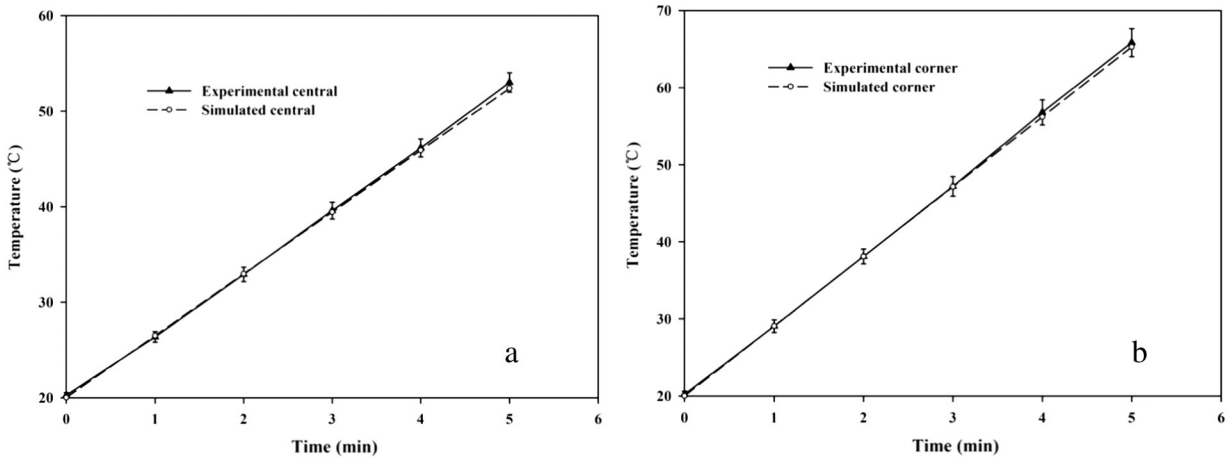

Fig. 8. Experimental and simulated temperature–time histories of soybean flour at the center (a) and corner (b) positions of middle layer ($z = 4$ cm), placed in a polystyrene container in the center and middle between the top and bottom electrodes during 5 min heating at a fixed electrode gap of 12 cm (bars indicate standard deviation of five runs).

was placed in the center and middle between the top and bottom electrodes. Fig. 6a–c corroborate the result as the maximum temperature values appeared at the corners and edges of all layers. In three horizontal layers, the temperature values were higher in the middle layer (51–74 °C), whereas they were lower in the top and bottom layers (50–68 °C and 52–67 °C). The highest temperature values occurred at the center parts of soybean flour over the volume, placed in the middle (3 cm above the bottom electrode) between two RF electrodes (Fig. 3). The non-uniform temperature distribution could be attributed to the electric field behavior, which was deflected at the sample corners and edges, resulting in higher temperature values at these parts (Fig. 6). These findings are corroborated by overheating at the edges and center parts of fish (Llave et al., 2015), raisins (Alfaifi et al., 2014), and wheat kernels (Jiao, Deng, et al., 2015) subjected to RF treatment.

3.3. Computer model validation

The simulated spatial temperature profiles of soybean flour over three layers were compared with the experimental results obtained using a thermal imaging camera (Fig. 7). Both results demonstrated that the experimental temperature distribution showed good agreement with the simulated data in the center parts of the top, middle, and bottom layers. For the corners and edges of the sample, the maximum temperature differences in the top, middle, and bottom layers were about 3, 4, and 2 °C, respectively. The temperature differences between experiment and simulation might be caused by the simplification of the RF units or ignored moisture and heat loss in the possible evaporation in the soybean flour samples. Fig. 8 shows the measured and simulated time–temperature profiles of soybean flour at center and corner positions (as demonstrated in Fig. 1). Both sets of data exhibited similar trends, with a heating rate of 5.2 °C/min for corner and 4.8 °C/min for center throughout the duration of the heating process. Acceptable RMSE values were obtained for corner (0.014 °C) and center (0.017 °C), respectively. Table 2 compares simulated and experimental average and standard deviation temperatures of all three layers after the 5 min RF heating. Five replicates of experimental average temperatures were slightly lower than those of the simulated ones, which were attributed to heat loss when samples were transferred from the RF cavity to the camera. The simulated standard deviations were comparatively higher than those determined by experiments. This was probably caused by more data points for corners with fine meshes in simulation, while these were equally distributed in the experiment. It was corroborated that the simulated temperature profile in all three layers could capture the actual temperature field variation, and the model accuracy could be guaranteed.

3.4. Effect of DPs of sample and container on sample temperature distribution

Fig. 9 shows electric field intensities in polystyrene container and soybean flour samples with container dielectric constant of 2.6 and 3.96, respectively. Simulated results illustrated how electric field patterns were distorted within the rectangular shaped sample. Severe edge heating usually happened at four corners and the bottom sections of sample–wall interfaces. When the dielectric constant differences between the surrounding material and treated sample was greater, deflection and distortion of the electric field increased more frequently at the contact surface of two different materials (Fig. 9a). The electric field distortion was reduced when the container dielectric constant changed to 3.96 (equal to the treated sample). The maximum electric field intensity decreased from 3.32 to 2.98 $\times$ 10^4 V m^{-1} over the whole treated sample and surrounding container (Fig. 9b). The top electrode voltage used in the simulation model was 4200 V determined by running multiple simulations with different inputted voltages until the target temperature (50 °C) was obtained at the top surface center (cold spot) of soybean flour (Jiao, Shi, et al., 2015). The maximum electric field difference of treated sample in the middle layer was reduced from 0.92 to 0.51 $\times$ 10^4 V m^{-1} after changing the dielectric constant of the surrounding container. The standard deviation of temperature and electric field at three horizontal layers of soybean flour was also reduced as shown in Table 3. Simulated UI of soybean flour decreased from 0.112 to 0.083 over the volume, demonstrating a rather uniform temperature obtained after 5 min RF heating. Therefore, different electric field patterns between surrounding container and food products could be minimized by appropriately matching DPs of the container with that of treated material.

Table 3
Simulated temperature (Ave ± SD, °C) and electric field intensity (Ave ± SD, V m^{-1}) of soybean flour in three different layers with container DPs of 2.6–0.0003·j and 3.96–0.0003·j under a fixed electrode gap of 12 cm.

Layer	Container DPs			
	2.6–0.0003·j		3.96–0.0003·j	
	Temperature (°C)	Electric field (V m^{-1})	Temperature (°C)	Electric field (V m^{-1})
Top	57.9 ± 4.4	18,886.2 ± 1488.4	59.3 ± 3.1	19,329.6 ± 923.3
Middle	59.6 ± 5.4	19,063.3 ± 1957.5	61.8 ± 4.3	20,125.4 ± 1226.5
Bottom	56.8 ± 3.8	17,151.9 ± 1019.7	58.1 ± 2.1	18,255.1 ± 864.4

3.5. Effect of DPs of sample and container on sample UI

Fig. 10a–c summarize the results of a series of simulations with surrounding container dielectric constant ranging from 0.1 to 19, and sample dielectric constants increasing progressively at regular intervals between 2 and 13, based on the previous measured DPs of soybean flour (Guo et al., 2010). Simulated results demonstrated that an increase in container dielectric constant caused initial reduction and then the increase of UI with the fixed sample dielectric constant values. UI was the lowest when the surrounding container dielectric constant was

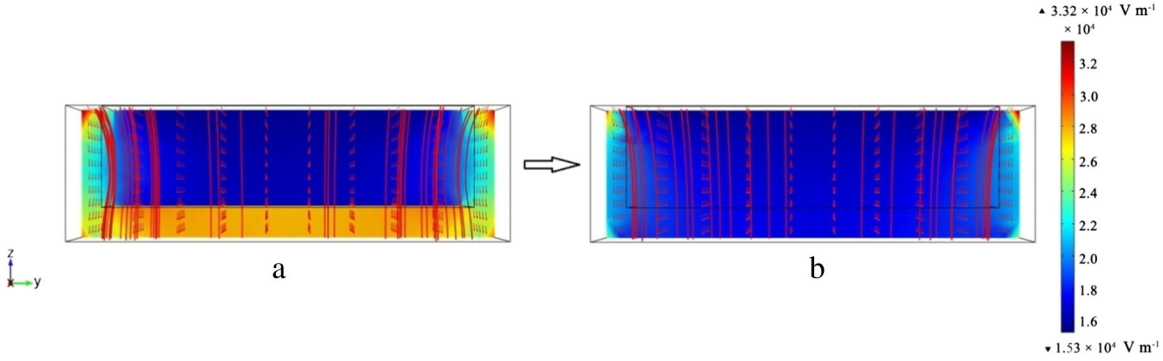

Fig. 9. Simulated electric field direction (arrow), electric field intensity (color surface, V m^{-1}), and electric potential (streamline) of soybean flour and polystyrene container with container DPs of (a) 2.6–j·0.0003 and (b) 3.96–j·0.0003 after 5 min RF heating under the fixed sample DPs of 3.96–j·0.38.

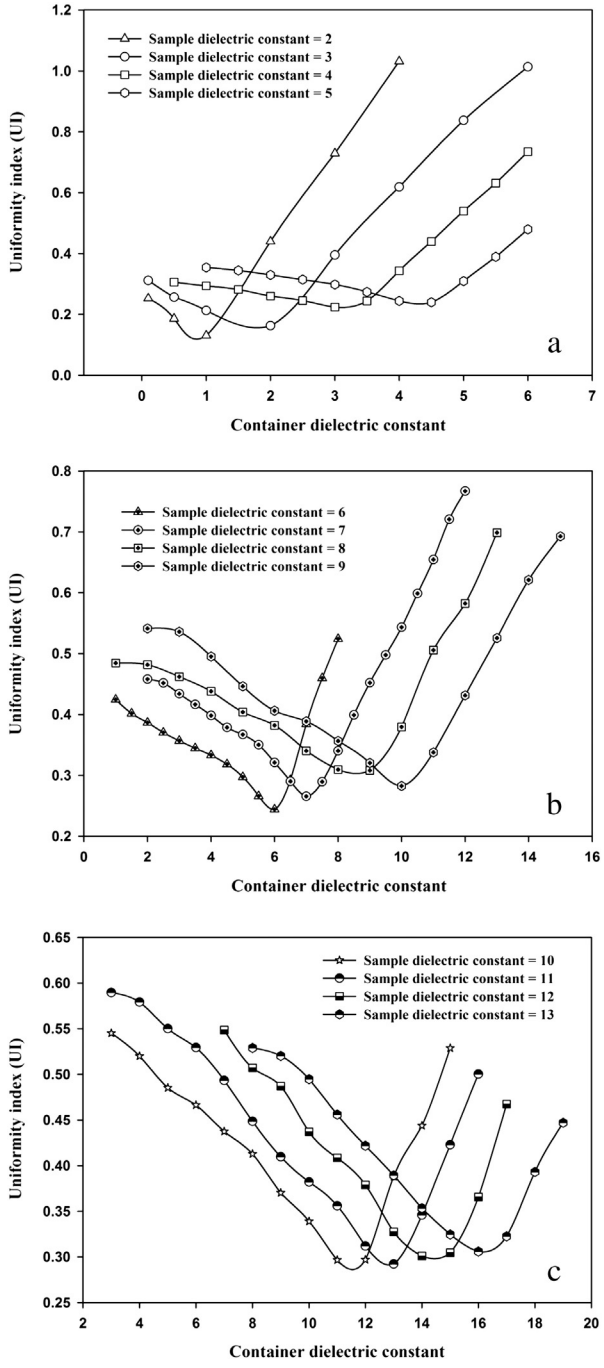

Fig. 10. Simulated UI of soybean flour with varying sample dielectric constants between (a) 2–5, (b) 6–9, and (c) 10–13 under various container dielectric constants after 5 min RF heating with an electrode gap of 12 cm.

smaller than that of the sample if dielectric constant of heated sample was <7. But for the dielectric constant of heated sample ≥ 7, UI started to get the minimal value when the surrounding container dielectric constant was greater than that of the sample. It was interesting to notice that UIs had their minimum values whenever the dielectric constants of surrounding container were in a comparable range with that of the sample. This was contrary to a general concept that increasing the dielectric constant of the surrounding container equal to that of the sample might obtain the best heating uniformity of the heated products. Logistic regression analysis was performed to determine the minimum values of UI by solving a set of quadratic equations based on the simulated trends of UI as illustrated in Fig. 10. Therefore, dielectric constants of the surrounding container could be determined by solving the roots of the regression equations. Table 4 shows the calculated dielectric constants of the surrounding container when the UI achieved the lowest values with various sample dielectric constants. The simulated voltages used in the computer simulation were in the range of 2860–9300 V in order to make the lowest temperature reach 50 °C. It is clear that trends of simulation voltage change depended on the dielectric constant of the sample and the surrounding container. Since the voltage level along the top electrode is proportional to the dielectric constant of the treated sample, it also increased with the increase in dielectric constant (Metaxas, 1996). The dielectric constant of the surrounding container as a function of that of the sample may be predicted according to the following regression equation with a high coefficient of determination ($R^2 = 0.99$):

$$\varepsilon'_{container} = 1.42\varepsilon'_{sample} - 2.54. \quad (8)$$

The predicted dielectric constant value of surrounding material was 8.8 with the DPs of wheat flour fixed as 8–10·j based on the developed regression equation. There was little difference with the literature findings that UI was the lowest when the surrounding material dielectric constant was between 8 and 11 (Tiwari et al., 2011a). The calculated dielectric constant value of surrounding sheets was 3.17 with DPs of peanut butter of 4.03–0.004·j. This was in good agreement with previous simulation results in which the RF heating uniformity was greatly improved by using the Polyetherimide (PEI) block (DPs of 3.15–0.0025·j) assisting method (Jiao, Tang, and Wang, 2014, Jiao, Shi, et al., 2015). Obviously, results demonstrated that the developed correlation equation is reliable for choosing the most suitable surrounding material to improve the RF heating uniformity in various food products. For example, the estimated dielectric constant value of surrounding container was 2.6 with dry soybean DPs of 3.6–0.26·j. This was in accordance with our preliminary studies that UI was the lowest when the surrounding material dielectric constant was between 2.5 and 3.5 (Huang, Zhu, Yan, et al., 2015). Optimum RF heating uniformity in other dry products (such as almond, lentil, wheat, walnut, pistachio nut, raisin, and rice) could be achieved with particular dielectric constant values of the surrounding material.

3.6. Effect of loss factor of sample and container on sample UI

Table 5 compares the simulated UIs of soybean flour with different loss factor values of surrounding container and heated sample. UI showed a sharp decrease first and then a constant as a function of container loss factor. The UI decreased from 5.052 to 0.244 when the loss factor of the surrounding container decreased from 0.3 to 0.00003 with a fixed sample loss factor of 0.1. It is also observed that when loss factor of sample increased gradually to 5, UI decreased from 0.472 to 0.321. UI was the lowest compared to other loss factor values when loss factors of the surrounding container were given between 0.00003 and 0.0003, 0.01–0.1% of the sample's one. Loss factor of sample describes the amount of electric energy converted to heat and the inputted voltages were lower when the sample loss factor decreased (Table 5). It is clear that the heating uniformity of food products could be improved when loss factors are small both for the surrounding container and

Table 4
The calculated dielectric constants of the surrounding container ($\varepsilon_{container}'$) when the UI obtained the minimum values and the corresponding inputted voltages (V) with varying sample dielectric constants (ε'_{sample}) in each simulation after 5 min RF heating.

ε'_{sample}	2	3	4	5	6	7
$\varepsilon'_{container}$	0.94	1.68	3.13	4.28	5.93	7.07
Simulation voltage (V)	2860	3540	4000	4490	5000	5600
ε'_{sample}	8	9	10	11	12	13
$\varepsilon'_{container}$	8.59	10.03	11.56	13.03	14.36	16.61
Simulation voltage (V)	6280	6820	7430	8060	8630	9300

Table 5
Simulated UI of soybean flour with varying loss factor values of sample (ε''_{sample}) and surrounding container ($\varepsilon''_{container}$) under the corresponding inputted voltages (V) after 5 min RF heating with an electrode gap of 12 cm.

ε''_{sample}	0.1					1				
$\varepsilon''_{container}$	0.3	0.03	0.003	0.0003	0.00003	0.3	0.03	0.003	0.0003	0.00003
UI	5.052	0.584	0.278	0.247	0.244	0.616	0.286	0.245	0.242	0.241
Simulation voltage (V)	9150	8000	8000	8000	8000	2580	2570	2560	2560	2560
ε''_{sample}	3					5				
$\varepsilon''_{container}$	0.3	0.03	0.003	0.0003	0.00003	0.3	0.03	0.003	0.0003	0.00003
UI	0.619	0.494	0.482	0.481	0.481	0.472	0.336	0.322	0.321	0.321
Simulation voltage (V)	1570	1570	1570	1570	1570	1670	1670	1670	1670	1670

treated samples (Huang, Zhu, and Wang, 2015). The UI may not be further reduced due to the small enough loss factor values of the polystyrene container (0.0003) used in this study. Therefore, the dielectric constant of surrounding container is the dominating factor to influence the heating uniformity of treated products. This behavior has been observed for dry soybeans (Huang, Zhu, Yan, et al., 2015), peanut butter (Jiao, Tang, and Wang, 2014, Jiao, Shi, et al., 2015), shell eggs (Lau, 2015), and wheat flour (Tiwari et al., 2011a) subjected to RF treatment.

3.7. Effect of density of sample and container on sample UI

Fig. 11 indicates that the smaller densities of surrounding container resulted in better RF heating uniformities within the samples. UI decreased slightly with increasing densities of the surrounding container but then increased dramatically under each fixed sample density values. Low densities of the surrounding container should provide a better heating uniformity due to the lower density values of heated material which resulted in higher RF heating rate (Huang, Zhu, and Wang, 2015). Table 6 shows the calculated density values of the surrounding container in each fixed sample density when the minimum values of UI were obtained. The inputted voltage increased with increasing sample density due to the positive correlation between sample density and top electrode voltage (Metaxas, 1996). Therefore, a linear relationship for densities of the surrounding container and treated products was observed with high coefficient of determination ($R^2 = 0.98$).

$$\rho_{container} = 0.36\rho_{sample} - 68.10. \quad (9)$$

It can be inferred from the above results that uniform RF heating of the sample could be achieved when the surrounding container density was far smaller than that of the sample. The regression equation developed in this study may be further used in other dry products and other

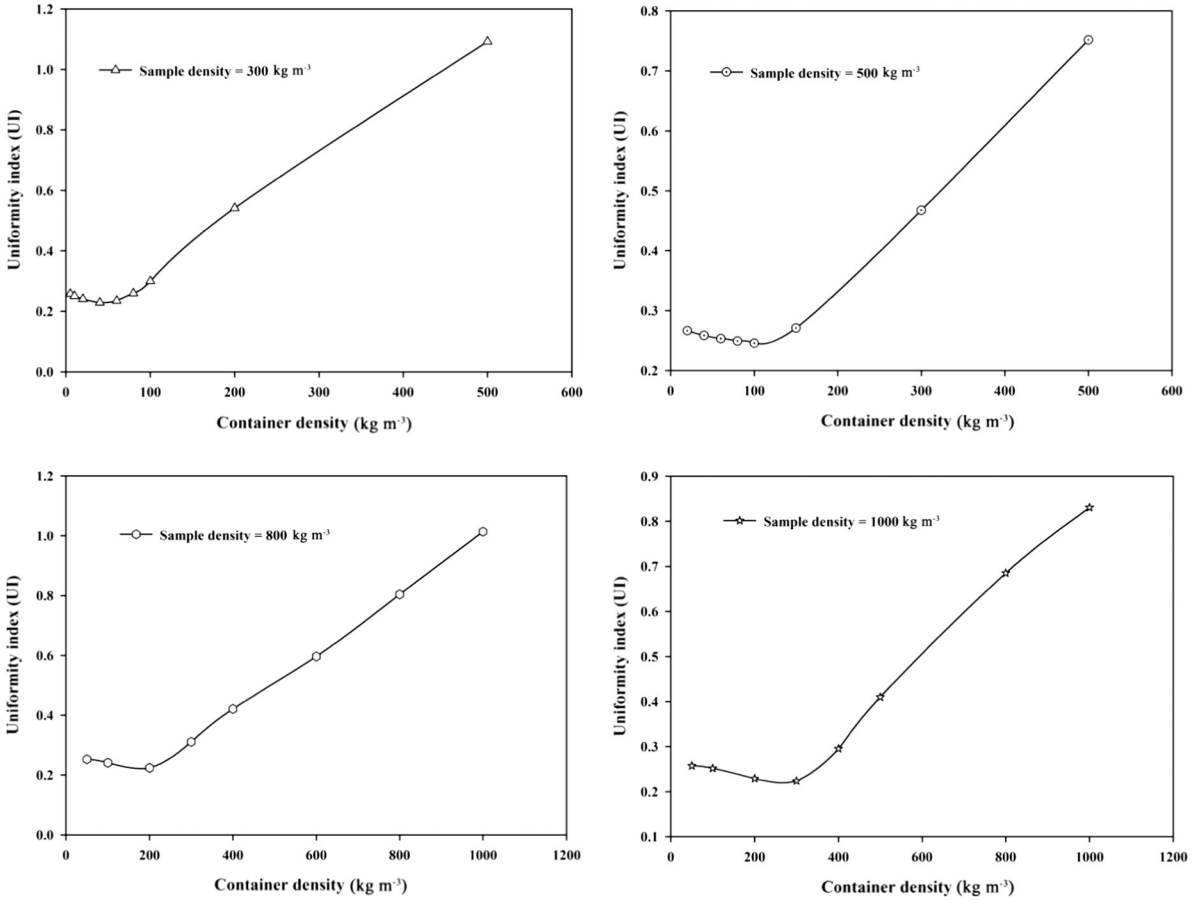

Fig. 11. Simulated UI of soybean flour with four different sample density values (300, 500, 800, and 1000 kg m^{-3}) and various container densities after 5 min RF heating with an electrode gap of 12 cm.

Table 6
The calculated density values of the surrounding container ($\rho_{container}$) when the UI reached the minimum values and the corresponding inputted voltages (V) with varying sample densities (ρ_{sample}) in each simulation after 5 min RF heating.

Sample density (ρ_{sample}, kg m^{-3})	300	500	800	1000
Container density ($\rho_{container}$, kg m^{-3})	50	100	210	300
Simulation voltage (V)	3560	4620	5780	6460

applications for heating uniformity improvement. Similar results have been also obtained by Huang et al. (2016) that the temperature uniformity was greatly improved by placing soybean samples in the polystyrene container (with low density) other than the polypropylene container. This suggests that the developed relationship could possibly be applied to other low moisture foods for overcoming edge heating effect and maintaining good product quality. Therefore, in practical applications for an industrial-scale RF system, which was equipped with an auxiliary hot air system and conveyor belt, choosing an optimum container material could be effectively minimize the effect of electric field bending and distortion within the corners and edges of food products during RF treatment. The developed correlation equations are a very effective tool for choosing the most suitable surrounding material to be used in an industrial application.

4. Conclusions

A comprehensive coupled electromagnetic and heat transfer model was developed by considering quasi-static electric fields in a 6 kW, 27.12 MHz RF heating system. Simulated temperature distribution in three horizontal layers of soybean flour was found in good agreement with experimental temperature profiles, except for some corners with maximum difference of 4 °C. The validated model was further used to study the effects of DPs and density of sample and surrounding container on sample UI. Simulated results illustrated that the RF heating uniformity could be improved when the dielectric constant and density of surrounding container and sample were in accordance with the established relationships. The smaller loss factor values for both surrounding container and heated products provided better temperature uniformities. The obtained regression equations may be useful to obtain a better heating uniformity in disinfestations of dry products and for designing an RF treatment protocol.

Acknowledgments

This research was conducted in the College of Mechanical and Electronic Engineering, Northwest A&F University, and supported by research grants from General Program of National Natural Science Foundation of China (31371853) and Program of Introducing International Advanced Agricultural Science and Technologies (948 Program) of Ministry of Agriculture of China (2014-Z21). The authors thank Qian Hao, Hongxue Zhou, Rui Li, Xiaoxi Kou, and Lixia Hou for their help in conducting the experiments.

References

Alfaifi, B., Tang, J., Jiao, Y., Wang, S., Rasco, B., Jiao, S., & Sablani, S. (2014). Radio frequency disinfestation treatments for dried fruit: Model development and validation. *Journal of Food Engineering, 120*, 268–276.

AOAC (2002). *Official methods of analysis*. Gaithersburg, MD, USA: Association of Official Analytical Chemists.

Ben-Lalli, A., Bohuon, P., Collignan, A., & Méot, J. M. (2013). Modeling heat transfer for disinfestation and control of insects (larvae and eggs) in date fruits. *Journal of Food Engineering, 116*(2), 505–514.

Birla, S., Wang, S., Tang, J., & Hallman, G. (2004). Improving heating uniformity of fresh fruit in radio frequency treatments for pest control. *Postharvest Biology and Technology, 33*(2), 205–217.

Chen, L., Wang, K., Li, W., & Wang, S. (2015). A strategy to simulate radio frequency heating under mixing conditions. *Computers and Electronics in Agriculture, 118*, 100–110.

COMSOL material library, COMSOL Multiphysics, V4.3a, (2012). Burlington, MA, USA

FAOSTAT (2013). Food and Agriculture Organization of the United Nations. Available at http://faostat.fao.org/site/312/default.aspx

Finn, S., Hinton, J. C., McClure, P., Amézquita, A., Martins, M., & Fanning, S. (2013). Phenotypic characterization of *Salmonella* isolated from food production environments associated with low water activity foods. *Journal of Food Protection, 76*(9), 1488–1499.

Fu, Y. C. (2004). Fundamentals and industrial applications of microwave and radio frequency in food processing. *Food Processing: Principles and applications* (pp. 79–100). Iowa, USA: Blackwell.

Gao, M., Tang, J., Villa-Rojas, R., Wang, Y., & Wang, S. (2011). Pasteurization process development for controlling *Salmonella* in in-shell almonds using radio frequency energy. *Journal of Food Engineering, 104*(2), 299–306.

Guo, W., Wang, S., Tiwari, G., Johnson, J. A., & Tang, J. (2010). Temperature and moisture dependent dielectric properties of legume flour associated with dielectric heating. *LWT-Food Science and Technology, 43*(2), 193–201.

Hassan, S. M. (2013). *Soybean, nutrition and health—Chapter 20*. Rijeka, Croatia, European Union: Intechopen access Publisher, 453–473.

Hou, L., Ling, B., & Wang, S. (2014). Development of thermal treatment protocol for disinfesting chestnuts using radio frequency energy. *Postharvest Biology and Technology, 98*, 65–71.

Huang, Z., Chen, L., & Wang, S. (2015). Computer simulation of radio frequency selective heating of insects in soybeans. *International Journal of Heat and Mass Transfer, 90*, 406–417.

Huang, Z., Zhu, H., & Wang, S. (2015). Finite element modelling and analysis of radio frequency heating rate in mung beans. *Transactions of the ASABE, 58*(1), 149–160.

Huang, Z., Zhu, H., Yan, R., & Wang, S. (2015). Simulation and prediction of radio frequency heating in dry soybeans. *Biosystems Engineering, 129*, 34–47.

Huang, Z., Zhang, B., Marra, F., & Wang, S. (2016). Computational modelling of the impact of polystyrene containers on radio frequency heating uniformity improvement for dried soybeans. *Innovative Food Science and Emerging Technologies* (in press).

Ikediala, J., Hansen, J., Tang, J., Drake, S., & Wang, S. (2002). Development of a saline water immersion technique with RF energy as a postharvest treatment against codling moth in cherries. *Postharvest Biology and Technology, 24*(2), 209–221.

Jiao, S., Deng, Y., Zhong, Y., Wang, D., & Zhao, Y. (2015). Investigation of radio frequency heating uniformity of wheat kernels by using the developed computer simulation model. *Food Research International, 71*, 41–49.

Jiao, S., Johnson, J., Tang, J., & Wang, S. (2012). Industrial-scale radio frequency treatments for insect control in lentils. *Journal of Stored Products Research, 48*, 143–148.

Jiao, Y., Shi, H., Tang, J., Li, F., & Wang, S. (2015). Improvement of radio frequency (RF) heating uniformity on low moisture foods with polyetherimide (PEI) blocks. *Food Research International, 74*, 106–114.

Jiao, Y., Tang, J., & Wang, S. (2014). A new strategy to improve heating uniformity of low moisture foods in radio frequency treatment for pathogen control. *Journal of Food Engineering, 141*, 128–138.

Jiao, Y., Tang, J., Wang, S., & Koral, T. (2014). Influence of dielectric properties on the heating rate in free-running oscillator radio frequency systems. *Journal of Food Engineering, 120*, 197–203.

Johnson, J., Wang, S., & Tang, J. (2003). Thermal death kinetics of fifth-instar *Plodia interpunctella* (Lepidoptera: Pyralidae). *Journal of Economic Entomology, 96*(2), 519–524.

Johnson, J., Wang, S., & Tang, J. (2010). Radio frequency treatments for insect disinfestation of dried legumes. *Proc.10th Intl. Working Conf. Stored Product Protection* (pp. 688–694). Berlin, Germany: Julius Kühn Institut.

Kim, S. Y., Sagong, H. G., Choi, S. H., Ryu, S., & Kang, D. H. (2012). Radio-frequency heating to inactivate *Salmonella* Typhimurium and *Escherichia coli* O157:H7 on black and red pepper spice. *International Journal of Food Microbiology, 153*(1), 171–175.

Lau, S. K. (2015). Simulation and validation of radio frequency heating of shell eggs. *Dissertations & Theses in Food Science and Technology, 61*, 1–133.

Llave, Y., Liu, S., Fukuoka, M., & Sakai, N. (2015). Computer simulation of radio frequency defrosting of frozen foods. *Journal of Food Engineering, 152*, 32–42.

Marra, F., Lyng, J., Romano, V., & McKenna, B. (2007). Radio-frequency heating of foodstuff: Solution and validation of a mathematical model. *Journal of Food Engineering, 79*(3), 998–1006.

Marshall, M., & Metaxas, A. (1998). Modeling of the radio frequency electric field strength developed during the RF assisted heat pump drying of particulates. *Journal of Microwave Power and Electromagnetic Energy, 33*(3), 167–177.

Metaxas, A. (1996). *Foundations of electroheat: A unified approach*. New York: John Wiley & Sons.

Mohapatra, D., Kar, A., & Giri, S. K. (2015). Insect pest management in stored pulses: an overview. *Food and Bioprocess Technology, 8*(2), 239–265.

Singh, P., Satya, S., & Naik, S. (2013). Grain storage insect–pest infestation-issues related to food quality and safety. *Internet Journal of Food Safety, 15*, 64–73.

Tiwari, G., Wang, S., Tang, J., & Birla, S. (2011a). Analysis of radio frequency (RF) power distribution in dry food materials. *Journal of Food Engineering, 104*(4), 548–556.

Tiwari, G., Wang, S., Tang, J., & Birla, S. (2011b). Computer simulation model development and validation for radio frequency (RF) heating of dry food materials. *Journal of Food Engineering, 105*(1), 48–55.

Uyar, R., Bedane, T. F., Erdogdu, F., Palazoglu, T. K., Farag, K. W., & Marra, F. (2015). Radio-frequency thawing of food products—A computational study. *Journal of Food Engineering, 146*, 163–171.

Vijay, S., Bhuvaneswari, K., & Gajendran, G. (2015). Assessment of grain damage and weight loss caused by *Sitophilus oryzae* (*L.*) feeding on split pulses. *Agricultural Science Digest, 35*(2), 111–115.

Wang, S., Tiwari, G., Jiao, S., Johnson, J., & Tang, J. (2010). Developing postharvest disinfestation treatments for legumes using radio frequency energy. *Biosystems Engineering, 105*(3), 341–349.

Zhu, H., Huang, Z., & Wang, S. (2014). Experimental and simulated top electrode voltage in free-running oscillator radio frequency systems. *Journal of Electromagnetic Waves and Applications, 28*(5), 606–617.